

# HEAT TRANSFER IN A TURBULENT CHANNEL FLOW WITH ROUGHNESS

**Stefano Leonardi**

Department of Mechanical Engineering,  
University of Puerto Rico at Mayaguez, Mayaguez, 00680, Puerto Rico, US  
sleonardi@me.uprm.edu

**Paolo Orlandi**

Dipartimento di Meccanica e Aeronautica,  
University of Rome "La Sapienza"  
via Eudossiana n. 18, 00184, Rome, Italy

**Robert A. Antonia**

Discipline of Mechanical Engineering,  
University of Newcastle, NSW 2308 Australia

## ABSTRACT

DNSs are carried out for passive heat transport in a turbulent channel flow with square bars on one wall. The total heat transfer depends on  $w/k$ , the pitch to height ratio of the roughness and it is maximum for  $w/k = 7$ . Instantaneous contours of streamwise velocity and scalar fluctuations are closely similar for  $w/k = 1$ . The mean temperature, scaled on wall units, has a slope which depends on  $w/k$ . The concept of a temperature roughness function is therefore questionable unless a virtual origin is used.

## INTRODUCTION

Turbulent transport of a passive scalar plays an important role in atmospheric flows. The passive scalar may be the temperature, humidity or some chemical species. The transport of pollution and heat out of the streets of a city into the overlying boundary layer is not understood sufficiently well and fluxes cannot be quantified with any degree of confidence. The scalar concentration at the street level is determined by the fluxes, and it is therefore important that these fluxes be quantified properly. In the atmospheric boundary layer, the surface is rough due to the buildings, hills and valleys. Coceal *et al.* (2006) and Orlandi & Leonardi (2006) analysed the flow field over an array of staggered and aligned cubes which mimic building blocks. Recently, Tseng *et al.* (2007) performed a LES of the flow field and the pollution concentration over a real city.

The study of turbulent heat or mass transport is of special interest in engineering, especially for heat exchangers. Kim & Moin (1989), Kasagi *et al.* (1992), Kawamura *et al.* (1999) studied the transport of a passive scalar in a turbulent channel flow with smooth walls. However, the surface of heat exchangers is deliberately rough. For instance, roughness elements (turbulators) are usually placed on the walls of the internal channels of a turbine blade to enhance the heat transfer (Han *et al.* 2000). Recently with the use of a cluster of computers, it has been possible to perform Direct Numerical Simulations (hereafter DNS) of the flow over a rough wall. Leonardi *et al.* (2003) studied how the pitch to height ratio of a square bar roughness influences the frictional and form drag and their correlation with the roughness function. Ashrafian *et al.* (2004) have performed a DNS of the turbu-

lent channel flow with a square bar roughness on both walls with a small  $k/h$  ratio. Bhaganagar *et al.* (2004) considered an egg-carton roughness underlying the differences between a 2D and a 3D roughness. Another kind of roughness has been recently studied by Ikeda & Durbin (2007) who considered square bar elements with different heights. Miyake *et al.* (2001) considered the transport of passive scalar over a rough wall. They studied the effect of square bars with  $w/k = 6$  ( $w$  is the spacing between roughness elements and  $k$  is the roughness height) on the temperature field. The roughness was simulated with a body force method, i.e. a force is added to the RHS of the Navier Stokes equation so that the velocity is equal to zero at the grid points relative to the roughness.

The present paper is an extension of Miyake's work and of Leonardi *et al.* (2003)'s parametric study. DNSs are carried out for passive heat transport in a turbulent channel flow with square bars on one wall. Several values of  $w/k$  are considered ( $w/k = 1, 3, 7, 11, 14, 29$ ). The Reynolds number  $Re = U_b h / \nu$  was set to 7000; here,  $U_b$  is the bulk velocity and  $\nu$  is the kinematic viscosity,  $h$  the channel half height. The computational box is  $6h \times 2.1h \times \pi h$  in  $x_1$  (streamwise),  $x_2$  (wall-normal) and  $x_3$  (spanwise direction) respectively (Fig.1). The additional  $0.1h$  increase in channel height corresponds to the cavity height where the square elements are placed. The plane of the crests is at  $x_2/h = -1$ . The instantaneous temperature ( $T$ ) is set to  $T = 1$  on the lower wall and to  $T = -1$  on the upper wall. The Prandtl number  $Pr$  is set equal to 1. The flow can be assumed to be "fully rough" since  $k^+$  ranges from about 40 for  $w/k = 1$  to about 80 for  $w/k = 7$ .

The dependence of the heat flux, temperature *rms* and correlation between temperature and velocity are discussed in the paper.

## NUMERICAL PROCEDURE

The non-dimensional Navier-Stokes and continuity equations for incompressible flows are:

$$\frac{\partial U_i}{\partial t} + \frac{\partial U_i U_j}{\partial x_j} = -\frac{\partial P}{\partial x_i} + \frac{1}{Re} \frac{\partial^2 U_i}{\partial x_j^2} + \Pi \delta_{i1}, \quad \nabla \cdot U = 0 \quad (1)$$

$\Pi$  is the pressure gradient required to maintain a constant

flow rate,  $\delta_{ij}$  is the Kronecher delta,  $U_i$  is the component of the velocity vector in the  $i$  direction and  $P$  is the pressure.

The energy equation is

$$\frac{\partial T}{\partial t} + \frac{\partial T U_j}{\partial x_j} = \frac{1}{Re Pr} \frac{\partial^2 T}{\partial x_j^2}, \quad (2)$$

where  $T$  is the temperature and  $Pr = \nu/\alpha$  is the Prandtl number, with  $\alpha$  the thermal diffusivity.

The Navier-Stokes and energy equations have been discretized in an orthogonal coordinate system using the staggered central second-order finite-difference approximation. Here, only the main features are recalled since details of the numerical method can be found in Orlandi (2000). The discretized system is advanced in time using a fractional-step method with viscous terms treated implicitly and convective terms explicitly. The large sparse matrix resulting from the implicit terms is inverted by an approximate factorisation technique. At each time step, the momentum equations are advanced with the pressure at the previous step, yielding an intermediate non-solenoidal velocity field. A scalar quantity  $\Phi$  projects the non-solenoidal field onto a solenoidal one. A hybrid low-storage third-order Runge-Kutta scheme is used to advance the equations in time. The roughness is treated by the efficient immersed boundary technique described in detail by Orlandi & Leonardi (2006). This approach allows the solution of flows over complex geometries without the need of computationally intensive body-fitted grids. It consists of imposing  $U_i = 0$  on the body surface which does not necessarily coincide with the grid. To avoid that the geometry is described in a stepwise way, at the first grid point outside the body, the second derivatives in the Navier Stokes equations are discretized using the distance between the velocities and the boundary of the body rather than using the mesh size.

## MEAN FLOW AND TEMPERATURE

Instantaneous contours of temperature are shown in Fig.1 superimposed on the time averaged streamlines. Leonardi *et al.* (2003) showed that the square bars on the bottom wall induce a separation at the trailing edge of the roughness elements. For  $w/k < 7$ , the reattachment is on the opposite vertical wall while for  $w/k \geq 7$ , the flow reattaches on the bottom wall upstream of the subsequent element, where a new separation region is formed. For  $w/k = 1$ , the flow almost skims the rough wall and the ejections of hot fluid out of the cavities resemble those on a smooth wall. Djenidi *et al.* (1999), using LDV, observed similar ejections out of 3 – 4 consecutive cavities. They speculated that this was caused by the passage of a streamwise vortex over the cavities. Leonardi *et al.* (2004) calculated 2D correlation contours with one point fixed on the wall for a range of  $w/k$ . For  $w/k = 1$ , they observed an inclination of the correlation contours similar to that of a smooth wall. As a consequence of the weak disturbance associated with this particular geometry, the temperature gradient in  $x_1$  does not vary much when compared to that at larger  $w/k$ . By increasing  $w/k$ , Leonardi *et al.* (2004) showed that the velocity contours increase their inclination with respect to the flow direction. This is due to the increased intensity of the wall-normal velocity fluctuations. The separated flow induces wall-normal velocities at the plane of the roughness crests which modify the structure of the overlying flow and enhance the mixing. In fact, Orlandi *et al.* (2006) showed that for various roughness shapes and densities the wall-normal velocity rms

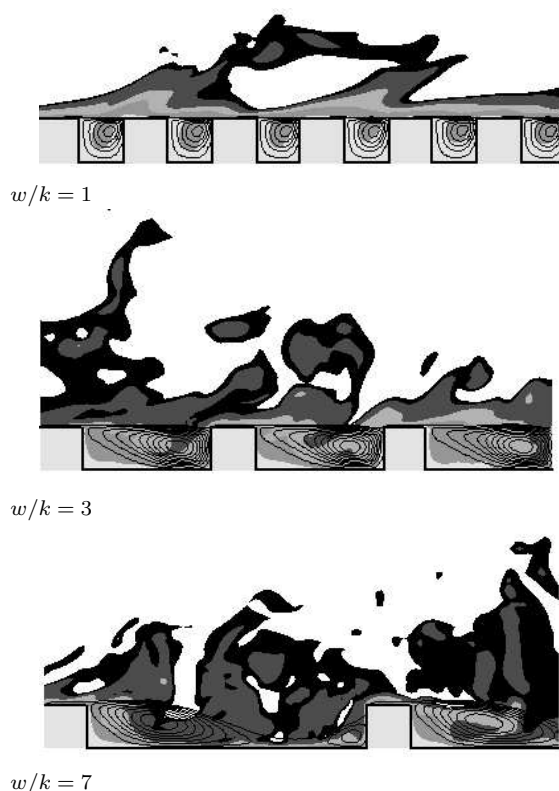


Figure 1: Geometrical sketch of the rough wall and color contours of temperature for  $w/k = 1, 3, 7$ . The rough wall (lower) is hot, the smooth (upper) cold. Contours from  $T = 1$  (light) to  $T = 0.6$  (dark) are shown.

is maximum in the range  $3 \leq w/k \leq 10$ . Temperature contours agree well with velocity correlation contours calculated in Leonardi *et al.* (2004). The instantaneous contours of temperature for  $w/k = 7$  shown in Fig.1 are almost perpendicular to the flow direction. The contour  $T = 0.6$  gives an approximate idea of how far the hot fluid extends away from the wall. For  $w/k = 7$ , the hot fluid penetrates more into the core of the flow. Therefore, the effect of the roughness on the overlying flow depends strongly on the roughness density. The case  $w/k = 3$  is intermediate presenting both vertical and inclined ejections.

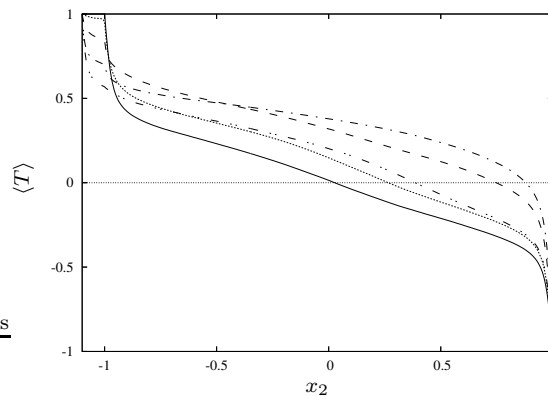


Figure 2: Mean temperature distribution: (—) smooth channel, (-----)  $w/k = 1$ , (----)  $w/k = 3$ , (— · —)  $w/k = 7$ , (— · — · —)  $w/k = 29$ .

A quantitative indication of the influence of roughness

on the mean temperature can be obtained by averaging the temperature with respect to time as well as streamwise and spanwise directions (Fig. 2).

With respect to the smooth wall channel, the roughness shifts the zero crossing of the temperature profile upward. This is due to the increase in heat transfer from the rough wall (hot) to the smooth wall (cold). For  $w/k = 7$ , the zero crossing is very close to the upper wall. The global temperature of the flow (i.e. the integral of the temperature over the whole domain  $T_t = \int_{-1}^1 \langle T \rangle dy$ ) increases as  $w/k$  increases, up to a maximum for  $w/k = 7$ , which is the most effective configuration for optimising the heat transfer. The temperature distribution for  $w/k = 29$  almost overlaps that for  $w/k = 1$ . This means that for large values of  $w/k$ , the flow behavior returns to that expected over a smooth wall.

### HEAT FLUX

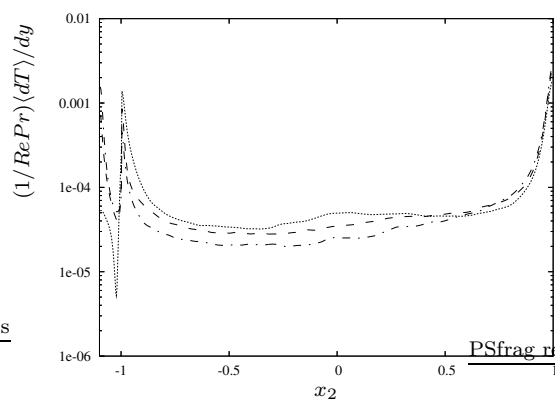


Figure 3: Mean temperature gradient distribution: (.....)  $w/k = 1$ , (-----)  $w/k = 3$ , (-.-.-)  $w/k = 7$ .

With respect to the smooth wall, the mean temperature gradient decreases in the inner part of the channel and increases on the upper smooth wall. At the crest plane, the mean temperature gradient decreases as the width of the cavity increases (Fig.3). The total heat transfer  $q$  is the sum of the molecular conduction ( $\frac{1}{PrRe} \frac{\partial \langle T \rangle}{\partial y}$ ) and of the turbulent heat flux  $-\langle Tv \rangle$ , (angular brackets denote averaging with respect to time as well as streamwise and spanwise directions,  $T$  is the instantaneous temperature and  $v$  is the wall-normal velocity fluctuation). Since the walls are isothermal, the heat flux has to be constant within the channel, i.e. all the heat transported from the hot wall has to exit from the upper wall. The turbulent heat flux increases as  $w/k$  increases with a maximum for  $w/k = 7$  (Fig.4). The distribution is constant with  $x_2$  across a large section of the channel, diminishing very near the wall where  $v = 0$ . For  $w/k = 3, 7$ , the heat transfer at the crest plane is almost entirely due to the wall-normal velocity fluctuations. In fact, the contribution from  $d\langle T \rangle / dy$  decreases with an increase in  $w/k$  (see Fig.3). The opposite occurs on the bottom wall, where  $v = 0$ , so that the heat transfer is associated with the gradient of  $\langle T \rangle$ . Consequently, on the bottom wall, for both  $w/k = 3$  and  $7$   $d\langle T \rangle / dy$  is steeper than over a smooth wall because the heat transfer is larger.

The variation of the molecular conduction and turbulent heat flux induce variation of the rms temperature distribution. The product  $-\langle Tv \rangle \partial \langle T \rangle / \partial y$  represents the production in the transport equation of the temperature variance. In a smooth wall channel, the temperature variance has three peaks, one on the centerline and the other two near the walls.

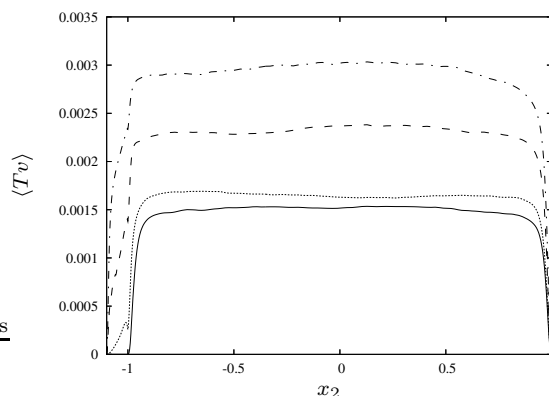


Figure 4: Turbulent heat flux averaged in time spanwise and streamwise directions: (————) smooth wall, (.....)  $w/k = 1$ , (-----)  $w/k = 3$ , (-.-.-)  $w/k = 7$ .

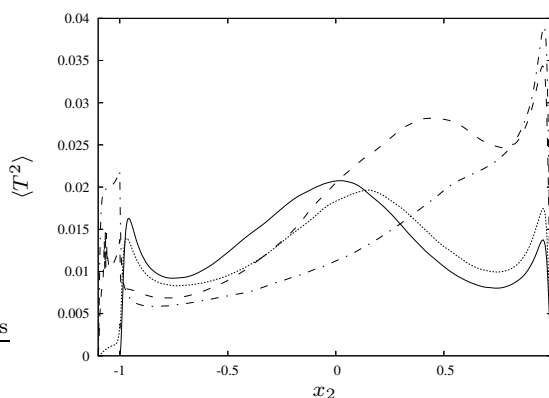


Figure 5: Temperature rms averaged in time spanwise and streamwise directions: (————) smooth wall, (.....)  $w/k = 1$ , (-----)  $w/k = 3$ , (-.-.-)  $w/k = 7$ .

For  $w/k = 1$ ,  $\langle T^2 \rangle$  is only slightly different from the smooth wall distribution. The peak at the centerline is shifted upward. In Fig.2 the zero crossing of the mean temperature was observed to be shifted towards the smooth wall. For  $w/k = 3$ , the peak of temperature rms increases and approaches the upper wall. For  $w/k = 7$ , only the two peaks near the walls can be observed. This is, in fact the case where the zero crossing of the mean temperature is closest to the upper wall. The temperature gradient is smallest in the inner channel and largest near the walls. As a consequence, for  $w/k = 7$ , the production term in the transport equation for  $\langle T^2 \rangle$  is large only near the walls and leads to a distribution very different from that over a smooth wall. If the temperature is thought as the concentration of a passive scalar, the small value of  $\langle T^2 \rangle$  near the crest plane means that the roughness can be used to improve the mixing.

To emphasize the effect the roughness has on  $\langle Tv \rangle$  and  $\frac{1}{RePr} d\langle T \rangle / Dy$  their value on the crests plane are shown as a function of  $w/k$  in Fig.6. Despite  $\langle Tv \rangle$  and  $\frac{1}{RePr} d\langle T \rangle / Dy$  vary as shown in Fig.3 and 4 their sum is constant with  $x_2$ . On the crest plane ( $x_2 = -1$ ), for small  $w/k$ , the molecular conduction dominates over the turbulent heat flux, while for large  $w/k$  the former is negligible with respect to the latter (Fig.6). The total flux is maximum for  $w/k = 7$  the configuration for which  $\langle v^2 \rangle$  is maximum (see Orlandi et al. 2006).

To understand how the roughness enhances the heat transfer, color contours of the vertical velocity rms in the

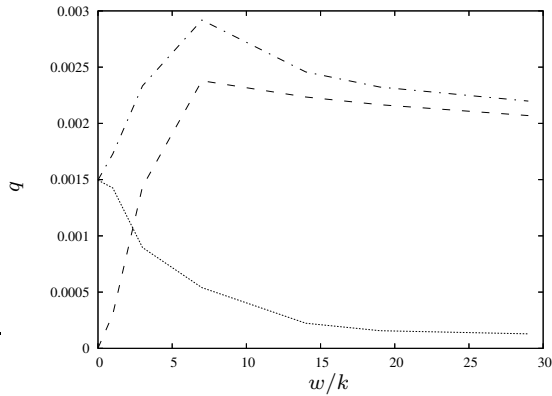


Figure 6: Dependence of the total heat flux (— · —), molecular conduction (·····) and turbulent heat flux (---) on  $w/k$ .

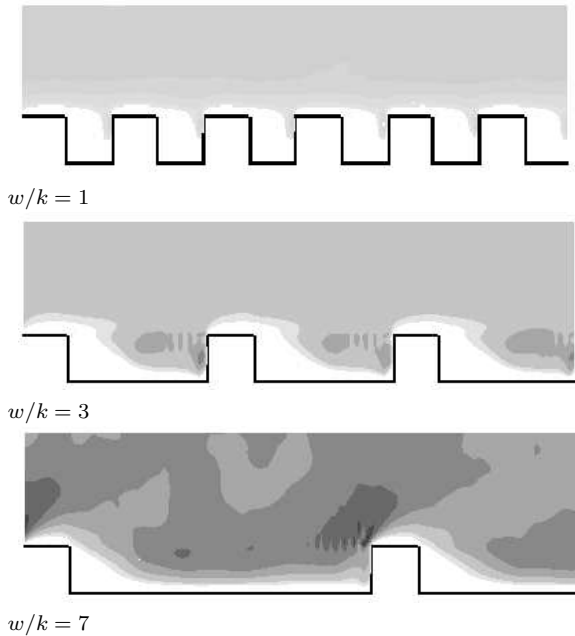


Figure 7: Color contours of  $\langle \nu_T \rangle$  averaged with respect to time and spanwise direction (dark high).

roughness layer are shown in Fig.7. Square cavities do not affect  $\langle \nu_T \rangle$  significantly. By increasing the width of the cavity, a waviness can be seen in the contours of  $\langle \nu_T \rangle$ . For  $w/k = 3$ , the largest values of  $\langle \nu_T \rangle$  can be observed within the cavity at about the crest plane. This may be due to the instability of the shear layer developing from the roughness crests and its interaction with the following element. For  $w/k = 7$ , an increase of  $\langle \nu_T \rangle$  similar to that for  $w/k = 3$  can be observed on the cavity. However, the impingement of the flow on the upstream wall of the element promotes large ejections. In this region, the intensity of  $\langle \nu_T \rangle$  is largest.

Because of the increased wall-normal velocity fluctuations, the heat is transported out of the wall into the core of the flow. Contours of  $\langle Tv \rangle$  are shown in Fig.8. There is a strong correspondence between  $\langle \nu_T \rangle$  and  $\langle Tv \rangle$  for  $w/k = 1$  and 3. In fact, for the latter, the turbulent heat flux is maximized near the leading edge of an element and on the top of the cavities. Although  $\langle \nu_T \rangle$  is approximately the same,  $\langle Tv \rangle$  is larger at the upstream wall of an element than at top of the cavity. This is because the temperature is larger at the

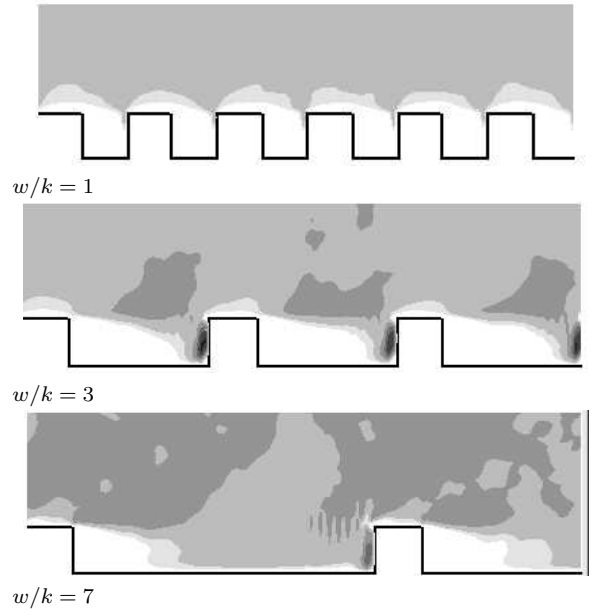


Figure 8: Color contours of  $\langle Tv \rangle$  averaged in time and spanwise direction (dark high).

leading edge (where  $T = 1$ ) than on the top of the cavity. For  $w/k = 7$ , the higher values of  $\langle Tv \rangle$  originate near the leading edge of the element and are then diffused for about half a wavelength. The streamwise variation of the heat flux may require a study of the temperature conduction within the solid walls. The present results are valid for highly conductive materials, while the conjugate heat transfer approach should be used when the conduction is small. Orlandi *et al.* (2007) have recently investigated the conjugate heat transfer on a turbulent channel flow for different materials. An inhomogeneous temperature within the material may cause structural problems.

The turbulent viscosity hypothesis assumes a correlation between  $d\langle u \rangle / dy$  and  $\langle uv \rangle$ . The ratio  $\nu_T = \langle uv \rangle / (d\langle u \rangle / dy)$  is the turbulent viscosity. Similarly, the gradient diffusion hypothesis is based on the correlation between  $d\langle T \rangle / dy$  and  $\langle Tv \rangle$  and the ratio  $\alpha_T = \langle Tv \rangle / (d\langle T \rangle / dy)$  is the turbulent diffusivity. The roughness increases both  $\langle uv \rangle$  and  $\langle Tv \rangle$  while the gradients of  $u$  and  $T$  decrease especially near the cavities. As a consequence both  $\nu_T$  and  $\alpha_T$  vary relative to a smooth wall channel (Fig.9). By increasing  $w/k$ ,  $\nu_T$  and  $\alpha_T$  increase due to the wall-normal velocity fluctuations. The larger increase is observed for  $w/k = 7$ . The effect of  $w/k$  on both  $\nu_T$  and  $\alpha_T$  extends far from the wall. Even at the centerline, the values of the turbulent viscosity and diffusivity are much larger than over a smooth wall. On a rough wall the strain is less important than in the case of a smooth channel. It appears that the signature of the rough wall is the wall-normal velocity distribution determined by the separations on the roughness elements and the instabilities of the shear layer. It seems also that the local disturbance on the rough wall, depending on the particular value of  $w/k$ , affects the flow even far from the wall. The turbulent Prandtl number  $Pr_T = \nu_T / \alpha_T$  is about 1.1 near the smooth wall (Antonia & Kim 1991). For a rough wall (Fig.9b) it increases near the crests plane, up to 2 for  $w/k = 7$ . This means that near the wall,  $\langle Tv \rangle$  dominates  $\langle uv \rangle$  while the opposite is observed in the inner part of the channel.

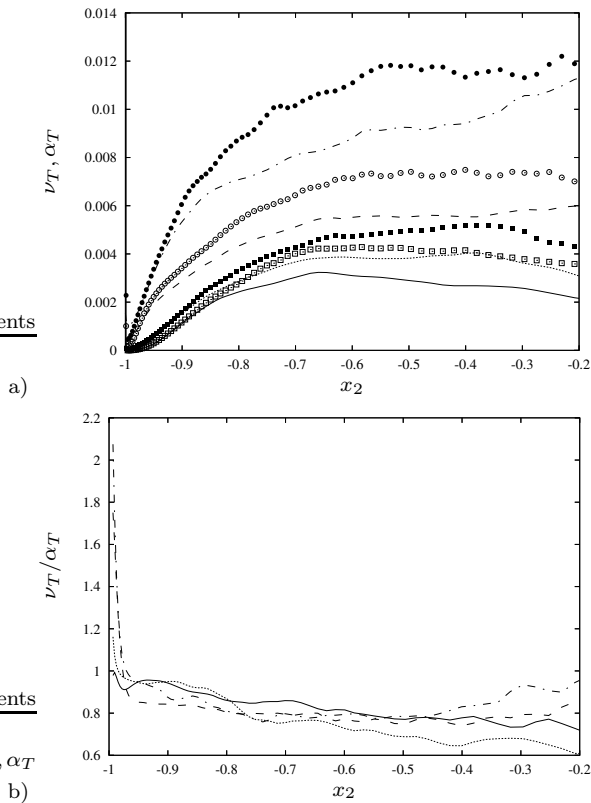


Figure 9: a) Turbulent viscosity (symbols) and gradient diffusion (lines), b) turbulent Prandtl number for (—)  $\square$  smooth wall, (·····)  $\blacksquare$   $w/k = 1$ , (----)  $\circ$   $w/k = 3$ , (— · —)  $\bullet$   $w/k = 7$ .

### SIMILARITY BETWEEN VELOCITY AND TEMPERATURE

There is a close similarity between  $u$  and  $T$  near a smooth wall and a strong correspondence of velocity and thermal streaks, (Iritani *et al.* 1985, Antonia *et al.* 1988, Kim & Moin 1989, Kasagi *et al.* 1992). Color contours of temperature are superimposed on contours of  $u$  fluctuations in Fig.10. For  $w/k = 1$ , there is a good correspondence between the two fields. High speed streaks, which are regions of high velocity fluid, correspond to colder fluid and vice versa. In fact, low speed streaks are associated with ejections of hot fluid with lower momentum. For  $w/k = 1$ , velocity and thermal streaks exhibits almost the same behaviour as over a smooth wall. For larger  $w/k$ , the coherence in  $x_1$  decreases and streaky structures are hardly observed. The correlation in  $x_3$  (spanwise direction) increases, then the structures are shorter and wider. The similarity between velocity and temperature still holds. This agree with the results of Orlandi & Leonardi (2004) who modeled a rough wall with the combination of an artificial smooth wall with wall-normal velocity disturbances taken from a simulation over a rough wall.

The mean temperature distribution on the smooth wall, scaled in wall units ( $\Delta T^+ = (\langle T \rangle - \langle T \rangle_c)/T^*$ , where  $\langle T \rangle_c$  is the mean temperature at the crest plane,  $T^* = q/U_\tau$ ,  $U_\tau = \sqrt{P_d + C_f}$ ,  $P_d$  is the pressure drag and  $C_f$  the frictional drag), overlaps the mean velocity distribution in the viscous sublayer and part of the log region (Fig.11). This is expected since for  $Pr = 1$  there is correspondence of the velocity and temperature equations (see also Orlandi & Leonardi 2004). For different values of  $Pr$ , the temperature and velocity distributions differ. The slope of the

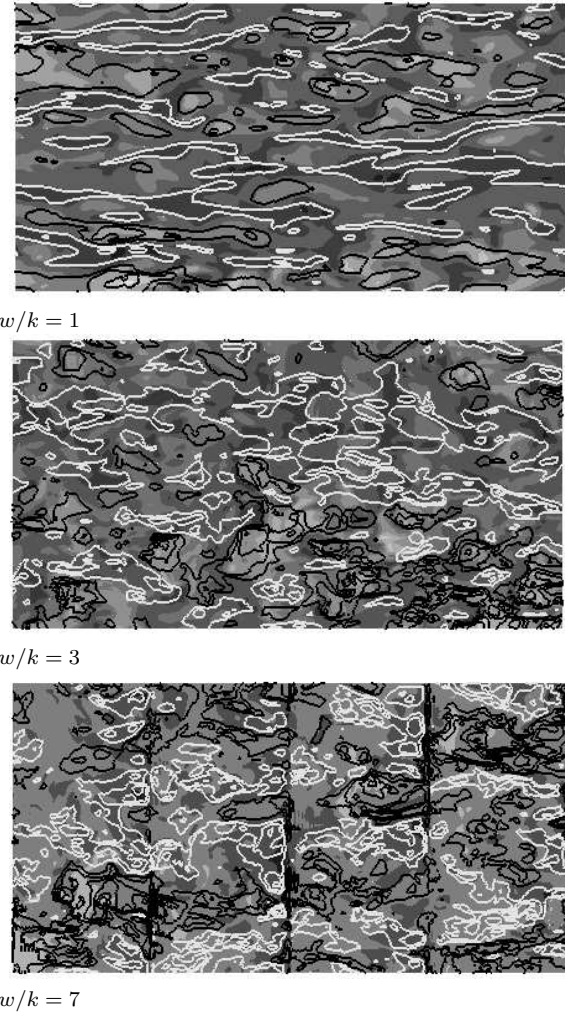


Figure 10: Color contours of temperature (dark high) superimposed to contour of streamwise velocity fluctuations (dark positive). The distance from the plane of the crests is about  $0.015h$  which corresponds to 6, 10 and 12 wall units for  $w/k = 1, 3, 7$  respectively.

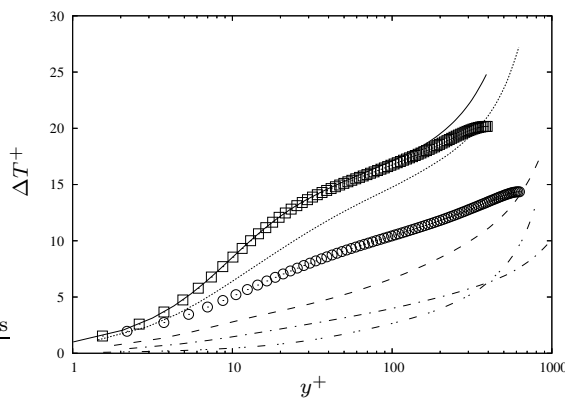


Figure 11: Temperature and velocity profiles in wall units on the rough wall. Lines, temperature legend as Fig.2. Symbols velocity profile:  $\square$  smooth wall,  $\circ$   $w/k = 1$ .

log-region depends strongly on  $Pr$  (Kawamura *et al.* 1999) On the other hand, on the rough surface, the mean temperature in wall units exhibits a downward shift with respect to

the smooth wall distribution which is similar to the velocity roughness function (Fig.11). This agrees with the results of Miyake *et al.* (2001) who, for  $w/k = 6$ , observed a downward shift of the temperature profile of about 6 wall units. However, the velocity and temperature profiles in wall units, do not overlap as for a smooth wall (Fig.11). Further the definition of the temperature roughness function is more ambiguous than that of the velocity roughness function since the slope of the mean temperature in the log region seems to depend on the value of  $w/k$ . Since roughness increases the turbulent Prandtl number, the slope of the log-region is expected to change. Another reason for the change in this slope is the origin in  $y$ . While for the velocity profiles a virtual origin is introduced to have a slope of the log-region equal to  $\kappa = 0.41$ , for the temperature profiles the origin is taken on the crest plane. If the same were done for the velocity profiles, a variation of the slope of the log-region would ensue. The maximum velocity roughness function is observed for  $w/k = 7$  (see Leonardi *et al.* 2003), the configuration for which  $U_\tau$  is maximum. Perhaps surprisingly, the maximum downward shift of the temperature profile is obtained for  $w/k = 29$  and not  $w/k = 7$  (for which the heat flux is maximum). In fact, on the crest plane,  $d\langle T \rangle/dy$  decreases as  $w/k$  increases (see Fig.6). It follows that, near the wall,  $\Delta T$  is smaller for  $w/k = 29$  than  $w/k = 7$ . The temperature is normalized by  $T^* = q/U_\tau$ . For  $w/k = 7$ , both  $q$  and  $U_\tau$  have maximum values; their ratio is 0.032. For  $w/k = 29$ , even if both  $q$  and  $U_\tau$  are smaller, their ratio  $T^* = 0.039$  is larger. The maximum downward shift is larger than for  $w/k = 29$ .

## CONCLUSION

The present simulations clearly demonstrate that roughness can be very effective in enhancing the turbulent (and total) heat transfer. The maximum heat flux occurs when  $w/k$  is equal to 7; this is the geometry for which the drag is maximum. While the velocity roughness function reflects the total drag, the temperature roughness function is not a good indicator of the total heat flux but is a measure of the ratio of the total heat flux to  $U_\tau$ . Since the slope of the temperature log-law depends on  $w/k$ , the temperature roughness function is not without ambiguity and cannot be relied upon on defining the heat transfer near a rough wall.

## ACKNOWLEDGMENTS

We acknowledge Dr. Amati for his help with the code optimization. We are also grateful to the super computer center "Caspur" ([www.caspu.it](http://www.caspu.it)) for the computational time available to us.

## REFERENCES

Antonia, R. A. & Kim, J. (1991) Turbulent Prandtl number in the near-wall region of a turbulent channel flow. *Int. J. of Heat and Mass Transfer* **34** 1905–1908.

Antonia R.A., Krishnamoorthy L.V. & Fulachier L. (1988) Correlation between the longitudinal velocity fluctuation and temperature fluctuation in the near-wall region of a turbulent boundary layer. *Int. J. of Heat and Mass Transfer*, vol. **31**, 723-730.

Ashrafian A., Andersson H. I. & Manhart M. (2004). DNS of turbulent flow in a rod-roughened channel. *Int. J. Heat and Fluid Flow*, **25**, 373-383.

Bhaganagar, K., Kim, J. & Coleman, G. (2004). Effect

of roughness on wall-bounded turbulence *Flow Turbulence and Combustion* **72**, 463–492.

Coccali O., Thomas T. G., Castro I. P., Belcher S. E. (2006) Mean flow and turbulence statistics over groups of urban-like cubical obstacles. *Boundary Layer Atm.* **121**, Number 3, 491-519.

Djenidi, L., Elavarasan, R. and Antonia, R.A. (1999). "The turbulent boundary layer over transverse square cavities". *J.Fluid Mech.* **395**, 271–294.

Ikeda T. & Durbin P.A. (2007) Direct simulations of a rough-wall channel flow *J. of Fluid Mech.*, 571: 235-263

Iritani, Y.; Kasagi, N.; Hirata, M. (1983) Heat transfer mechanism and associated turbulence structure in the near-wall region of a turbulent boundary layer. Symposium on Turbulent Shear Flows, 4th, Karlsruhe, West Germany.

Kasagi, N., Tomita, Y. & Kuroda, A., (1992) Direct numerical simulation of passive scalar field in a turbulent channel flow. *Trans. ASME* **114** 598-606.

Kawamura, H., Abe, H. and Matsuo, Y., (1999). DNS of turbulent heat transfer in channel flow with respect to Reynolds and Prandtl number effect. *Int. J. Heat Fluid Flow* **20** 1962-1977.

Kim J. & Moin P. (1989). Transport of passive scalars in a turbulent channel flow. *Turbulent Shear Flows 6*. Springer Verlag, Berlin 85-96

Han, J.C., Dutta, S. & Ekkad S. (2000) Gas Turbine Heat Transfer and Cooling Technology. *Taylor & Francis*.

Leonardi, S., Orlandi, P., Smalley, R.J., Djenidi, L. & Antonia, R.A. (2003). Direct numerical simulations of turbulent channel flow with transverse square bars on one wall. *J. Fluid Mech.* **491**, 229-238.

Leonardi, S., Orlandi, P., Djenidi, L. & Antonia, R.A. (2004) Structure of turbulent channel flow with square bars on one wall. *Int. J. Heat and Fluid Flow*, **25**, 384–392, 2004.

Miyake Y., Tsujimoto K. & Nakaji M. (2001) Direct numerical simulation of a rough-wall heat transfer in a turbulent channel flow. *J. Heat Fluid Flow* **22**:237–244.

Orlandi, P. (2000) Fluid flow phenomena, a numerical toolkit. *Kluwer Academic Publishers*.

Orlandi P. & Leonardi S. (2004) Passive Scalar in a Turbulent Channel Flow with Wall Velocity Disturbances. *Flow Turb. Comb.* **72**, 181-197

Orlandi P. & Leonardi S. (2006) DNS of turbulent channel flows with two- and three-dimensional roughness. *Journal of Turbulence*, **7**.

Orlandi P., Leonardi S. & Antonia R.A. (2006) Turbulent channel flow with either transverse or longitudinal roughness elements on one wall, *J. Fluid Mech.* **561** 279–305.

Orlandi P., Leonardi S. & Amati G. (2007) Conjugate heat transfer in a turbulent channel flow. *Turbulent Shear Flow Phenomena*, Munich.

Tseng, Y.H., Meneveau C., & Parlange M.B. (2006) Modeling Flow around Bluff Bodies and Predicting Urban Dispersion Using Large Eddy Simulation. *Environ. Sci. Technol.*, **40** (8), 2653 -2662.